Bimetallic Nanocrystals

DOI: 10.1002/ange.201106899

Convex Polyhedral Au@Pd Core–Shell Nanocrystals with High-Index Facets**

Dongheun Kim, Young Wook Lee, Sang Bok Lee, and Sang Woo Han**

The morphology-controlled synthesis of metal nanocrystals (NCs) has been an attractive research area for the past decade, especially in the field of catalysis, because the NC shape can significantly influence the catalytic activity and stability of the NCs in a variety of chemical reactions.[1–4] Exposed NC surface facets with a specific morphology, which can vary with the NC shape, may be responsible for the catalytic activity. Recently, the synthesis of NCs bound by high-index facets has been of particular interest because these high-index facets usually show catalytic properties that are enhanced relative to those of low-index facets because of the high concentration of catalytically active atomic steps and kinks.[5] The successful preparation of monometallic tetrahexahedral (THH), trisoctahedral (TOH), and concave cubic NCs enclosed by high-index facets has been achieved by electrochemical and wet chemical methods.[6–16] However, synthetic approaches to preparing high-index facets in bimetallic NCs have not been explored as extensively as in monometallic NCs. Very recently, limited success has been achieved in the preparation of bimetallic NCs with high-index facets. Using a seed-mediated synthetic method, Huang and co-workers prepared Au@Pd core–shell THH NCs from cubic Au seeds.[17] High-index faceted Pd shells were also formed through the heteroepitaxial growth of Pd layers onto THH and TOH Au NCs.[18,19]

Considering that bimetallic NCs display catalytic properties that are more pronounced than those of their monometallic counterparts, and their properties depend strongly on morphology, as in the case of monometallic NCs,[20] tailoring the shape of bimetallic NCs to include high-index facets can endow them with novel catalytic functions. In previous work, we showed that Au–Pd bimetallic alloy or core–shell NCs with various shapes can be prepared by the judicious control of NC nucleation and growth kinetics.[21–27] These results prompted us to examine the possibility that bimetallic NCs enclosed by high-index facets could be generated by manipulating the reaction conditions. Here, we describe the synthesis of high-index-faceted Au@Pd core–shell NCs with an unprecedented convex polyhedral shape through the co-reduction of Au and Pd precursors in the presence of octahedral Au NC seeds. The prepared NCs were predominantly enclosed by high-index {12 5 3} facets. Electrocatalysis experiments unambiguously showed that high-index-faceted convex polyhedral Au@Pd core–shell NCs displayed much higher catalytic activity and stability compared with cubic and octahedral Au@Pd core–shell NCs bound by low-index {100} and {111} facets, respectively.

In a typical synthesis of convex Au@Pd core–shell NCs, $HAuCl_4$ (10 mM, 0.3 mL), K_2PdCl_4 (10 mM, 0.2 mL), and L-ascorbic acid (100 mM, 2 mL) were added to an aqueous solution (20 mL) of octahedral Au NCs (0.12 mM_{Au}; see the Supporting Information for details). Octahedral Au NC seeds with an average edge length of 35 nm were prepared according to a previously reported procedure (see Figure S1 in the Supporting Information).[28] The mixture was gently shaken, then left undisturbed at room temperature for about 2 h. Figure 1a shows a representative scanning electron microscopy (SEM) image of the sample (see also the low-magnification SEM image shown in Figure S2 in the Supporting Information), revealing the formation of NCs with hexoctahedron-like structures. The NCs could be prepared in high yield (> 85%). The average NC size was (47 ± 3) nm, estimated from the distance between neighboring NC apices. An SEM image of a tilted sample further displayed that the NCs included eight pods and six small protrusions (Figure 1b). These observations, together with high-magnification SEM images of NCs in different orientations (Figure 1c), supported the geometric model shown in Figure 1c. This structure was consistent with a growth model in which the NCs formed by growth of eight hexagonal pyramids on a rhombic dodecahedron surface along the ⟨111⟩ direction (the violet region in the geometric model), leaving the six vertices of the rhombic dodecahedron intact (the pink region in the geometric model).

In the structural model, eight hexagonal pyramidal pods of the NCs assume a hexoctahedron-like structure. A common hexoctahedral (HOH) structure is a polyhedron bound by 48 triangular high-index {*hkl*} ($h > k > l > 0$) facets (Table S1 in the Supporting Information).[18] In contrast with

[*] Y. W. Lee, Prof. S. W. Han
Department of Chemistry and KI for the NanoCentury, KAIST
Daejeon 305-701 (Korea)
E-mail: sangwoohan@kaist.ac.kr
Homepage: http://ntl.kaist.ac.kr
D. Kim, Prof. S. B. Lee
Graduate School of Nanoscience and Technology (WCU)
KAIST, Daejeon 305-701 (Korea)
E-mail: slee@umd.edu
Prof. S. B. Lee
Department of Chemistry and Biochemistry
University of Maryland, College Park, MD 20742 (USA)

[**] This work was supported by the National Research Foundation (NRF) funded by the Korean government (MEST) through Basic Science Research Programs (grant number 2010-0029149), the WCU Program (grant number R31-2008-000-10071-0), the EPB Center (grant number 2008-0062042), and the Future-based Technology Development Program (Nano Fields; grant number 2009-0082640).

Supporting information for this article is available on the WWW under http://dx.doi.org/10.1002/anie.201106899.

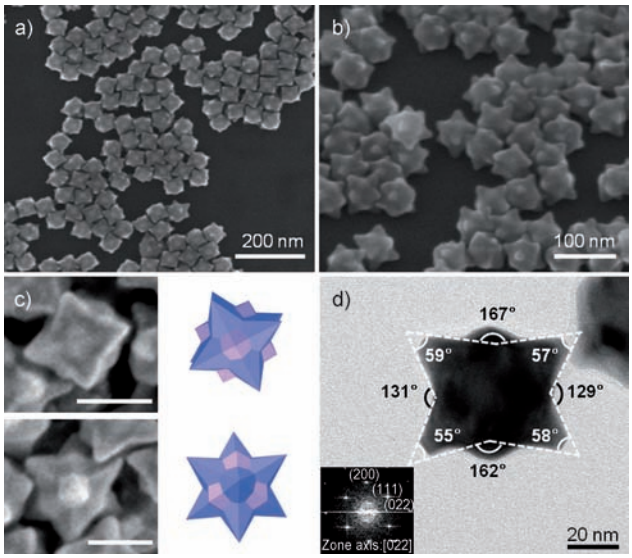

Figure 1. a) Typical SEM image of convex polyhedral Au@Pd NCs. b) SEM image of NCs tilted by 45°. c) SEM images and corresponding geometric model of NCs in different orientations. The scale bars indicate 50 nm. d) TEM image of a single convex polyhedral Au@Pd NC viewed along the ⟨110⟩ direction. The corresponding FFT pattern is shown in the bottom-left inset.

the common HOH shape, the hexagonal pyramidal pods of NCs were HOH structures with ⟨111⟩ edges that were elongated along the ⟨111⟩ direction. The Miller indices of the exposed facets of the NCs were estimated from the angles between the facets.[5] Figure 1 d shows a transmission electron microscopy (TEM) image of a NC viewed along the ⟨110⟩ direction. The corresponding fast Fourier transform (FFT) pattern shown in the inset indicates a $[0\bar{2}2]$ zone axis. The projection angles measured from the TEM image agreed well with the theoretically predicted values for the {12 5 3} facets (see Table S1 in the Supporting Information), suggesting that the prepared NCs were enclosed predominantly by {12 5 3} facets. The TEM images of NCs oriented along the different directions also gave the identical result (see Figure S3 in the Supporting Information). The high-index facets of the face-centered cubic (fcc) crystals could be represented in the "microfacet notation" as a combination of low-index facets from which the relative sizes of the terraces, steps, and kinks on the high-index surfaces could be identified.[29] The {12 5 3} facet of the NCs could be decomposed into $[7_7(100)+3_6(111)+2_2(110)]$, indicating the presence of (100) terraces with seven unit cells, (111) steps with six unit cells, and (110) kinks with two unit cells. The relative sizes of the terraces, steps, and kinks, with respect to the number of atoms, are 7, 3, and 2, respectively. The high-index surfaces of *fcc* crystals could also be denoted as $n(hkl)_t \times (hkl)_s$ according to the "step notation", reflective of the fact that $(hkl)_t$ terraces of n atomic width are separated by single-height $(hkl)_s$ steps.[29] This step notation has been widely used to identify the structures of high-index stepped surfaces because it can be correlated with the atomic arrangements observed in high-resolution TEM (HRTEM) images of the edge-on facets of NCs.[5–19] The {12 5 3} facet of the NCs could be expressed in the step notation as $7(100)\times(553)$, indicating that the step itself was a high-index (553) plane, a kinked step, as revealed by the microfacet notation. Therefore, the Miller indices of the exposed surfaces of the NCs could not be determined from the arrangement of atoms in the two-dimensionally projected HRTEM images of NCs.[18] The exposed facets of six small square pyramidal protrusions of NCs were expected to be {110} because they are the intact vertex regions of the rhombic dodecahedron.[30] This can be supported by the projection angles measured from the TEM image of NCs viewed along the different directions (see Figure S3 in the Supporting Information).

Elemental mapping of Au and Pd (Figure 2 a) and the compositional line profiles of a NC (Figure 2 b) obtained by high-angle annular dark-field scanning TEM-energy dispersive X-ray spectroscopy (HAADF-STEM-EDS) showed that the NCs had a core–shell structure consisting of a Au core and a Pd shell. The average thickness of the Pd shell on the side faces and tips of the hexoctahedron-like arms were 1.9 and 4 nm, respectively, whereas the rhombic dodecahedral protrusions had a thin Pd shell with an average thickness of 1.6 nm (Figure 2 c–f). The site-dependent thickness of the Pd layers was ascribed to the different growth rates along each

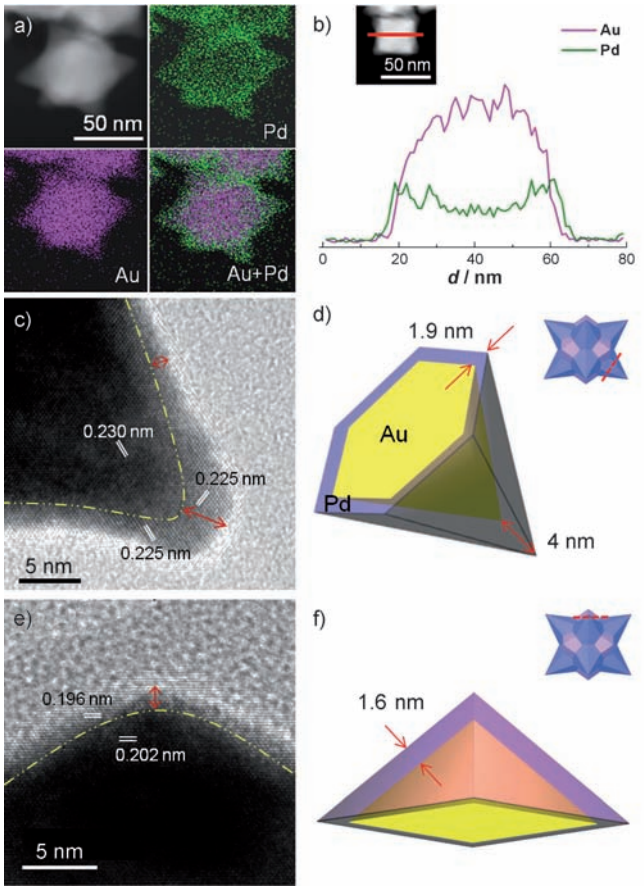

Figure 2. a) HAADF-STEM-EDS mapping images of the convex Au@Pd NCs. b) HAADF-STEM image and cross-sectional compositional line profiles of a convex Au@Pd NC (d = distance). c) TEM image and d) cross-sectional model of a hexoctahedron-like arm in a convex Au@Pd NC. e) TEM image and f) cross-sectional model of a rhombic dodecahedral protrusion of a convex Au@Pd NC.

growth direction. Indeed, metals preferentially deposited on the surfaces of growing seeds along the ⟨111⟩ direction such that the thickest Pd layers formed on the tip areas of the hexoctahedron-like arms. The Au/Pd molar ratio in the NCs was estimated to be 76.7:23.3 based on the relative volume, density, and atomic weight of each metal in the core–shell structure (see Table S2 in the Supporting Information). The calculated value was similar to that measured by inductively-coupled plasma-atomic emission spectrometry (ICP-AES), 76.3:23.7. The X-ray diffraction (XRD) pattern of the NCs showed distinct diffraction peaks from the fcc structure of the metal, indicating that the prepared NCs were crystalline (see Figure S4 in the Supporting Information). Because the reduction potential of Au^{3+} is higher than that of Pd^{2+}, the formation of Au@Pd core–shell NCs under our experimental conditions was most likely initiated by the preferential reduction of Au ions on the octahedral Au NC seeds, followed by the deposition of a Pd layer.[21,22]

The growth mechanism of convex Au@Pd NCs was investigated by examining the structural evolution of NCs as a function of the reaction time. Figure 3 shows TEM images

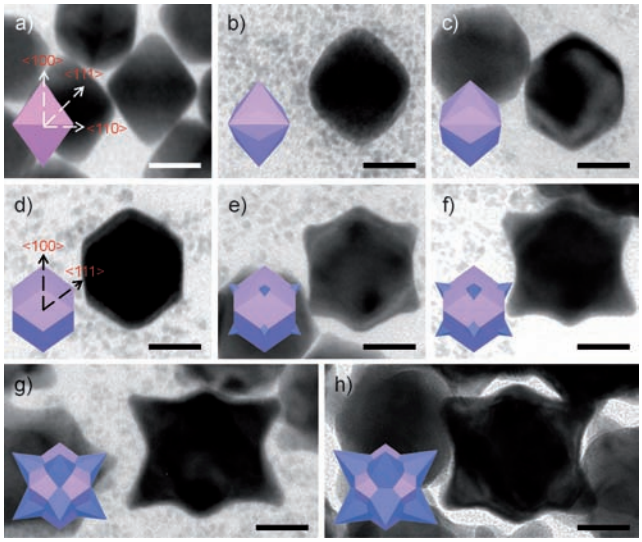

Figure 3. TEM images and corresponding geometric models of NCs prepared with different reaction times: a) 0, b) 0.5, c) 1, d) 2, e) 3, f) 5, g) 10, and h) 20 min. The scale bars indicate 20 nm.

and structural models of NCs prepared with different reaction times (see also the low-magnification TEM images in Figure S5 in the Supporting Information). Within 2 min NCs with a rhombic dodecahedral shape were grown from the octahedral NC seeds (Figure 3a–d). The exposed facets of rhombic dodecahedral NCs are {110} (see Figure S6 in the Supporting Information). After 3 min of reaction small pods were formed on the eight vertices of the rhombic dodecahedron (Figure 3e). By further increasing the reaction time, the pods grew in size and elongated along the ⟨111⟩ direction of the rhombic dodecahedron, eventually yielding hexoctahedron-like arms (Figure 3f–h). It is worth noting that the six vertices of the rhombic dodecahedron that pointed toward the ⟨100⟩ direction were intact during the growth of NCs (pink regions in the structural models). Beyond 20 min no significant change in structure was observed. The structural evolution was also reflected in the distinct UV/Vis spectral changes in the reaction mixture (see Figure S7 in the Supporting Information). These observations confirmed that octahedral NC seeds transformed into rhombic dodecahedral NCs, and finally into convex NCs with hexoctahedron-like arms through the preferential deposition of metals onto the surfaces of the growing seeds along the ⟨111⟩ direction.

Varying the Au/Pd molar ratio showed that the Au/Pd ratio in the precursor solution was critical to the formation of convex Au@Pd NCs. NCs grown from octahedral NC seeds using only $HAuCl_4$ or K_2PdCl_4 as a metal precursor resulted in rhombic dodecahedral or cubic shapes, respectively (see Figure S8a and S8f in the Supporting Information). When mixed metal precursors with Au/Pd ratios of 4:1, 3:2, 1:1, and 2:3 were used, NCs with hexoctahedron-like arms were generated (Figure 1 and Figure S8b-d in the Supporting Information), whereas the use of metal precursors with a Au/Pd ratio of 1:4 did not yield hexoctahedron-like armed NCs (see Figure S8e in the Supporting Information). On the other hand, the sequential reduction of Au and Pd precursors onto Au NC seeds produced rhombic dodecahedral Au@Pd NCs instead of convex Au@Pd NCs (see Figure S9 in the Supporting Information). These findings indicated that the co-reduction of both metal precursors in a suitable molar ratio was indispensable for the successful formation of convex Au@Pd NCs. This can be attributed to the competitive reduction between Au and Pd precursors, which can modulate the growth kinetics of NCs.[26,31,32] Moreover, an adequate amount of reducing agent, ascorbic acid, was required to realize convex Au@Pd NCs. Convex Au@Pd NCs were produced only from solutions containing ascorbic acid in a concentration higher than 50 mM (see Figure S10 in the Supporting Information). Cetyltrimethylammonium bromide (CTAB), which was used as a surfactant in the preparation of octahedral Au NC seeds and remained present in the seed solutions, could form a Au^{III}–CTAB complex during the synthesis of NCs. This complex might oxidize the Au seeds. However, the possible oxidation of Au NC seeds from a Au^{III}–CTAB complex has a negligible influence on the shape evolution of the NCs under our experimental conditions (see Figure S11 in the Supporting Information).

Au–Pd bimetallic alloy and core–shell NCs have been widely studied because of their excellent catalytic efficiencies for a variety of chemical reactions.[33] In particular, Pd-based catalysts provide a higher electrocatalytic activity toward ethanol oxidation than Pt in alkaline solutions.[34] To show a morphologic advantage of the convex Au@Pd NCs in catalysis, their electrocatalytic performance toward ethanol oxidation was investigated and the results were compared with the performance of other type of high-index-faceted Au@Pd core–shell NCs such as HOH Au@Pd NCs enclosed by high-index {431} facets as well as with those of cubic and octahedral Au@Pd NCs that had low-index {100} and {111} facets on their surfaces, respectively. The HOH, cubic, and octahedral Au@Pd NCs were prepared according to previously reported protocols (experimental details and Figure S12 in the Supporting Information).[18,22] Figure 4a shows cyclic

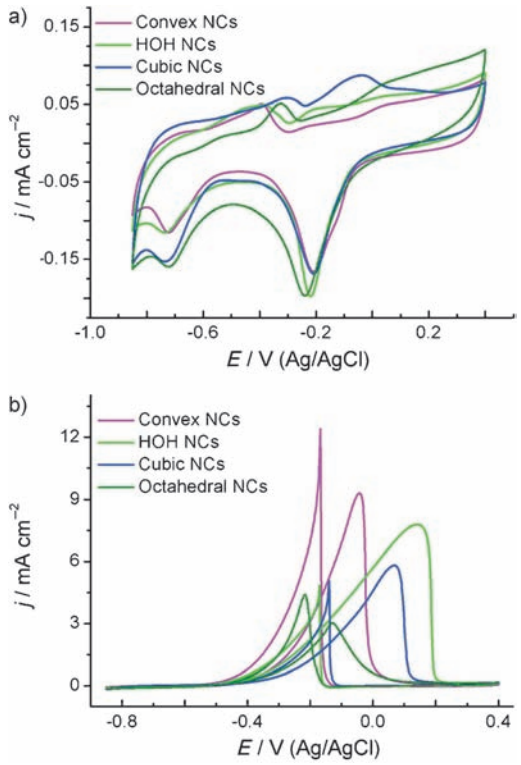

Figure 4. CVs of GCE modified with four different Au@Pd NCs obtained in a) 0.1 M KOH and b) 0.1 M KOH + 0.5 M ethanol solution at a scan rate of 50 mV s^{-1}. The current values were normalized with respect to the ECSA.

voltammograms (CVs) of glassy carbon electrodes (GCEs) modified with NCs obtained in a 0.1 M KOH solution at a scan rate of 50 mV s^{-1}. Typical current peaks associated with the oxidation/reduction of Pd were observed. The current densities were normalized to the electrochemically active surface areas (ECSA).[35] During the cathodic sweep, the peak for the reduction of Pd oxide appeared around −0.2 V versus Ag/AgCl for convex Au@Pd NCs, of which the peak position was similar to those of other Au@Pd NCs, and even identical to that of cubic Au@Pd NCs. This further indicates that the shell of convex Au@Pd NCs consists of pure Pd. Figure 4b shows the ethanol oxidation activities of four different NCs obtained in a 0.1 M KOH with 0.5 M ethanol solution. Well-separated anodic peaks in the forward and reverse sweeps, associated with the oxidation of ethanol, were identified. As shown in Figure 4b, the convex polyhedral Au@Pd NCs showed a peak current density of 9.3 mA cm^{-2} in the forward scan, higher than those of HOH (7.7 mA cm^{-2}), cubic (5.8 mA cm^{-2}), and octahedral (3.0 mA cm^{-2}) Au@Pd NCs. Moreover, the mass activity of convex Au@Pd NCs was highest among the various Au@Pd NCs (see Figure S13a in the Supporting Information). Chronoamperometry (CA) experiments at −0.1 V versus Ag/AgCl also showed that the electrochemical stability of convex Au@Pd NCs toward ethanol electrooxidation was superior to those of the other Au@Pd NCs (see Figure S13b in the Supporting Information), indicating that high-index NC facets of convex Au@Pd NCs promote catalytic stability as well as catalytic activity in the context of electrooxidation reactions.

The higher electrocatalytic activity of convex Au@Pd NCs compared with those of low-index-faceted Au@Pd NCs as well as high-index-faceted HOH Au@Pd NCs can result from the presence of relatively large amounts of catalytically active atomic steps and kinks. On the other hand, it can be assumed that the different catalytic performances of the various Au@Pd NCs may also be due to a difference in the modification of the electronic structure of Pd shells by Au cores. It has been reported that a charge redistribution between core and shell metals in core–shell NCs owing to different work functions between constituent metals can modulate the adsorption strength of reaction intermediates onto the NC surfaces, thus the redistribution determines the overall catalytic activity of the NCs.[36] Recently, Tsang and co-workers have shown that the rate of a catalytic reaction with M@Pd core–shell nanocatalysts (M = Au, Ag, Rh, Ru, and Pt) increases as the extent of charge transfer from cores to Pd shells increases because of the increase of adsorption strength of the intermediates.[37,38] To examine the electronic structure of Pd shells in the various Au@Pd NCs, binding energies for Pd 3d of the NCs were obtained by X-ray photoelectron spectroscopy (XPS). The Pd 3d binding energies of four different Au@Pd NCs follow the order convex < HOH < cubic < octahedral NCs, and an excellent linear relationship is found between the Pd 3d binding energy and the maximum current density for ethanol oxidation of the NCs (see Figure S14 in the Supporting Information). In fact, there is no correlation between Pd 3d binding energy and the Pd shell thickness of NCs. From these results, it can be inferred that the highest catalytic activity of convex Au@Pd NCs among the various Au@Pd NCs is the result of the large charge transfer from the Au core to the Pd shell together with the large number of catalytically active sites relative to those of the other Au@Pd NCs.

In summary, convex polyhedral Au@Pd core–shell NCs enclosed predominantly by high-index {12 5 3} facets were synthesized under aqueous room-temperature conditions through simultaneous reduction of Au and Pd ions in the presence of octahedral Au NC seeds. The NCs evolved from octahedral NC seeds to form first rhombic dodecahedral NCs and then hexoctahedron-like NCs through the preferential deposition of metals onto the growing seed surfaces along the ⟨111⟩ direction. The convex Au@Pd NCs showed electrocatalytic properties towards ethanol oxidation that were distinctly higher than those of the other Au@Pd NCs. Because the synthesized high-index-faceted NCs display unique structural and catalytic properties, they will find applications as materials for the fabrication of novel nanostructures and the development of efficient fuel cells.

Received: September 28, 2011
Published online: November 18, 2011

Keywords: electrocatalysis · ethanol · gold · nanocrystals · palladium

[1] Y. Xia, Y. Xiong, B. Lim, S. E. Skrabalak, *Angew. Chem.* **2009**, *121*, 62; *Angew. Chem. Int. Ed.* **2009**, *48*, 60.
[2] C. Burda, X. Chen, R. Narayanan, M. A. El-Sayed, *Chem. Rev.* **2005**, *105*, 1025.
[3] Z. Peng, H. Yang, *Nano Today* **2009**, *4*, 143.
[4] Y. W. Lee, M. Kim, S. W. Han, *Chem. Commun.* **2010**, *46*, 1535.
[5] N. Tian, Z.-Y. Zhou, S.-G. Sun, *J. Phys. Chem. C* **2008**, *112*, 19801.
[6] N. Tian, Z.-Y. Zhou, S.-G. Sun, Y. Ding, Z. L. Wang, *Science* **2007**, *316*, 732.
[7] Y. Ma, Q. Kuang, Z. Jiang, Z. Xie, R. Huang, L. Zheng, *Angew. Chem.* **2008**, *120*, 9033; *Angew. Chem. Int. Ed.* **2008**, *47*, 8901.
[8] T. Ming, W. Feng, Q. Tang, F. Wang, L. Sun, J. Wang, C. Yan, *J. Am. Chem. Soc.* **2009**, *131*, 16350.
[9] N. Tian, Z.-Y. Zhou, N.-F. Yu, L.-Y. Wang, S.-G. Sun, *J. Am. Chem. Soc.* **2010**, *132*, 7580.
[10] J. Li, L. Wang, L. Liu, L. Guo, X. Han, Z. Zhang, *Chem. Commun.* **2010**, *46*, 5109.
[11] D. Y. Kim, S. H. Im, O. O. Park, *Cryst. Growth Des.* **2010**, *10*, 3321.
[12] H.-L. Wu, C.-H. Kuo, M. H. Huang, *Langmuir* **2010**, *26*, 12307.
[13] Y. Yu, Q. Zhang, X. Lu, J. Y. Lee, *J. Phys. Chem. C* **2010**, *114*, 11119.
[14] J. Zhang, M. R. Langille, M. L. Personick, K. Zhang, S. Li, C. A. Mirkin, *J. Am. Chem. Soc.* **2010**, *132*, 14012.
[15] T. Yu, D. Y. Kim, H. Zhang, Y. Xia, *Angew. Chem.* **2011**, *123*, 2825; *Angew. Chem. Int. Ed.* **2011**, *50*, 2773.
[16] X. Huang, Z. Zhao, J. Fan, Y. Tan, N. Zheng, *J. Am. Chem. Soc.* **2011**, *133*, 4718.
[17] C.-L. Lu, K. S. Prasad, H.-L. Wu, J. A. Ho, M. H. Huang, *J. Am. Chem. Soc.* **2010**, *132*, 14546.
[18] Y. Yu, Q. Zhang, B. Liu, J. Y. Lee, *J. Am. Chem. Soc.* **2010**, *132*, 18258.
[19] F. Wang, C. Li, L.-D. Sun, H. Wu, T. Ming, J. Wang, J. C. Yu, C.-H. Yan, *J. Am. Chem. Soc.* **2011**, *133*, 1106.
[20] R. Ferrando, J. Jellinek, R. L. Johnston, *Chem. Rev.* **2008**, *108*, 845.
[21] Y. W. Lee, N. H. Kim, K. Y. Lee, K. Kwon, M. Kim, S. W. Han, *J. Phys. Chem. C* **2008**, *112*, 6717.
[22] Y. W. Lee, M. Kim, Z. H. Kim, S. W. Han, *J. Am. Chem. Soc.* **2009**, *131*, 17036.
[23] Y. W. Lee, M. Kim, Y. Kim, S. W. Kang, J.-H. Lee, S. W. Han, *J. Phys. Chem. C* **2010**, *114*, 7689.
[24] S. W. Kang, Y. W. Lee, M. Kim, J. W. Hong, S. W. Han, *Chem. Asian J.* **2011**, *6*, 909.
[25] J. W. Hong, Y. W. Lee, M. Kim, S. W. Kang, S. W. Han, *Chem. Commun.* **2011**, *47*, 2553.
[26] Y. W. Lee, M. Kim, S. W. Kang, S. W. Han, *Angew. Chem.* **2011**, *123*, 3528; *Angew. Chem. Int. Ed.* **2011**, *50*, 3466.
[27] J. W. Hong, D. Kim, Y. W. Lee, M. Kim, S. W. Kang, S. W. Han, *Angew. Chem.* **2011**, *123*, 9038; *Angew. Chem. Int. Ed.* **2011**, *50*, 8876.
[28] D. Kim, J. Heo, M. Kim, Y. W. Lee, S. W. Han, *Chem. Phys. Lett.* **2009**, *468*, 245.
[29] M. A. Vanhove, G. A. Somorjai, *Surf. Sci.* **1980**, *92*, 489.
[30] G. H. Jeong, M. Kim, Y. W. Lee, W. Choi, W. T. Oh, Q.-H. Park, S. W. Han, *J. Am. Chem. Soc.* **2009**, *131*, 1672.
[31] Y. Liu, A. R. H. Walker, *Angew. Chem.* **2010**, *122*, 6933; *Angew. Chem. Int. Ed.* **2010**, *49*, 6781.
[32] C. J. DeSantis, A. A. Peverly, D. G. Peters, S. E. Skrabalak, *Nano Lett.* **2011**, *11*, 2164.
[33] G. J. Hutchings, *Chem. Commun.* **2008**, 1148.
[34] C. Bianchini, P. K. Shen, *Chem. Rev.* **2009**, *109*, 4183.
[35] The ECSA were estimated by the following equation, ECSA = Q_o/q_o, where Q_o is the surface charge that can be obtained from the area under the CV trace of reduction of a metal oxide, and q_o is the charge required for desorption of a monolayer of oxygen on the Pd surface (424 $\mu C\,cm^{-2}$).
[36] J. X. Wang, H. Inada, L. Wu, Y. Zhu, Y. M. Choi, P. Liu, W.-P. Zhou, R. R. Adzic, *J. Am. Chem. Soc.* **2009**, *131*, 17298.
[37] K. Tedsree, C. W. A. Chan, S. Jones, Q. Cuan, W.-K. Li, X.-Q. Gong, S. C. E. Tsang, *Science* **2011**, *332*, 224.
[38] K. Tedsree, T. Li, S. Jones, C. W. A. Chan, K. M. K. Yu, P. A. J. Bagot, E. A. Marquis, G. D. W. Smith, S. C. E. Tsang, *Nat. Nanotechnol.* **2011**, *6*, 302.

